



Supplement of

Formation of condensable organic vapors from anthropogenic and biogenic volatile organic compounds (VOCs) is strongly perturbed by NO_x in eastern China

Yuliang Liu et al.

Correspondence to: Wei Nie (niewei@nju.edu.cn)

The copyright of individual parts of the supplement might differ from the article licence.

Table of contents

S1 Diurnal pattern of mass spectra of nitrate CI-APi-TOF and related parameters	1
S2 PMF inputs and diagnostics	1
S3 Calculation of molecular properties of OOMs.....	7
S4 Main peaks of 9 discussed non-nitrated-phenols factors	8
S5 The dependence of Temp-related factor on temperature.....	13
S6 Air masses reaching the SORPES station	15
S7 High resolution peak fitting	16

S1 Diurnal pattern of mass spectra of nitrate CI-APi-TOF and related parameters

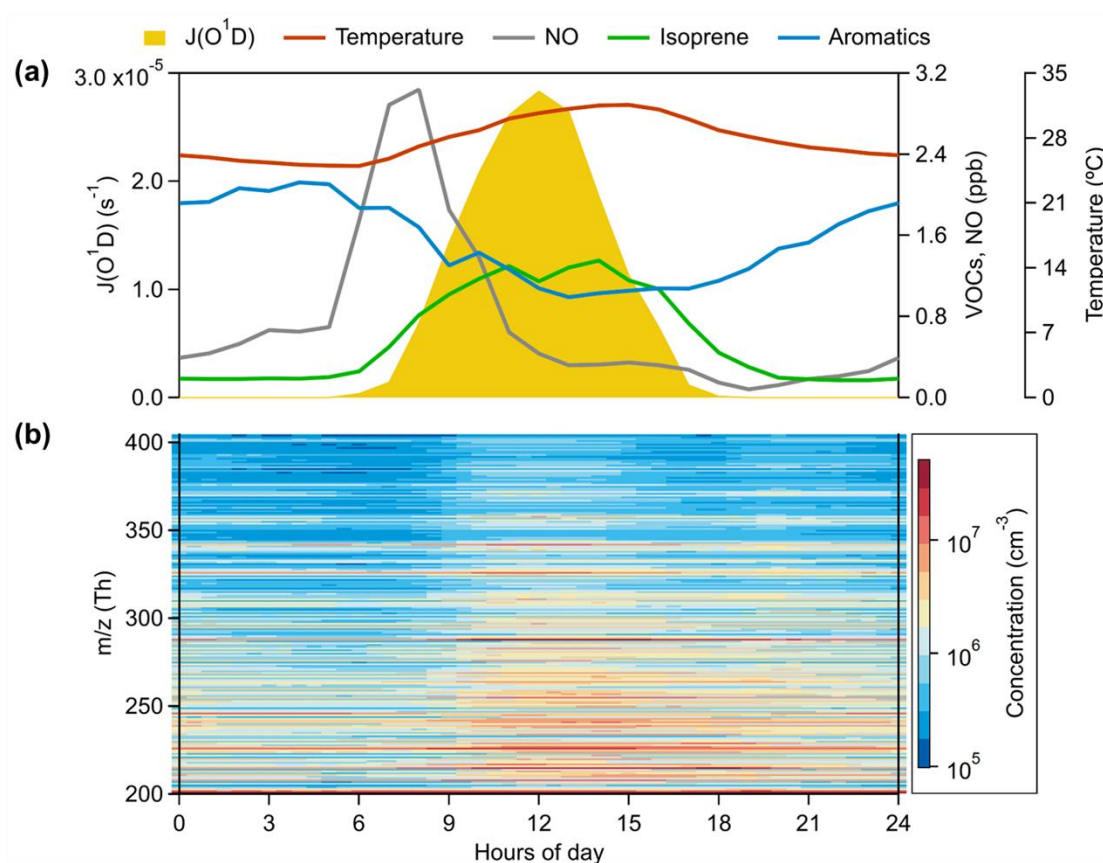


Fig. S1. Median diurnal variations of (a) $J(O^1D)$, Temperature, NO, total aromatics (benzene + toluene + C_8 aromatics + C_9 aromatics + C_{10} aromatics + styrene), and isoprene, and (b) mass spectra of nitrate CI-APi-TOF with m/z in the range of 201-404 Th.

S2 PMF inputs and diagnostics

S2.1 binPMF inputs

Data matrix

In binPMF, as described in Zhang et al. (2019), the mass spectra are divided into small bins of 0.006 Th width after baseline subtraction and mass axis calibration. Figure S1 (b) shows the averaged binned spectrum measured by nitrate CI-APi-TOF. We deleted bins of nitrophenol and some fluorinated contaminations (Table S1) from the raw spectra. The concentration of nitrophenol ($C_6H_5NO_3(NO_3^-)$) is about one order of magnitude higher than other compounds, but it is not our main concern. Fluorinated contaminations come from Teflon tube volatiles and perfluoric acid for mass dependent transmission efficiency calibrations, so these artificially introduced compounds with high signals should also not be taken into the PMF model. To avoid unnecessary computation, for each nominal m/z in the range of 202-404 Th, only signal regions with signal-to-noise ratio >1 were adopted as data matrix for PMF inputs.

Table S1. Peak list of deleted bins

Mass-to-charge (Th)	Formulas
201.0153	$C_6H_5NO_3(NO_3^-)$
207.9875	$C_2F_4HCOOH(NO_3^-)$
225.9780	$C_2F_5COOH(NO_3^-)$
241.9730	$C_3F_5OCOOH(NO_3^-)$
262.9760	$C_4F_9COO^-$
275.9748	$C_3F_7COOH(NO_3^-)$
307.9811	$C_4F_8HCOOH(NO_3^-)$
325.9716	$C_4F_9COOH(NO_3^-)$
341.9666	$C_4F_9OCOOH(NO_3^-)$
362.9696	$C_6F_{13}COO^-$
375.9685	$C_5F_{11}COOH(NO_3^-)$

Error matrix

The error matrix was calculated based on Eq. (1) (Polissar et al., 1998)

$$S_{ij} = \sigma_{ij} + \sigma_{noise} \quad (1)$$

where S_{ij} represents the uncertainty of m/z_j at time i and σ_{ij} stands for counting statistics uncertainty and is estimated as follows:

$$\sigma_{ij} = a \times \frac{\sqrt{I_{ij}}}{\sqrt{t}} \quad (2)$$

where I is the signal intensity term, in unit of ions per second; t stands for length of averaging in seconds, and a is an empirical coefficient to compensate for unaccounted

uncertainties (Allan et al., 2003; Yan et al., 2016) and is 1.28 in this study as previously estimated from laboratory experiments (Yan et al., 2016). The σ_{noise} term was estimated as the median of the standard deviations from signals in the bins in the region between nominal masses, where no physically meaningful signals are expected.

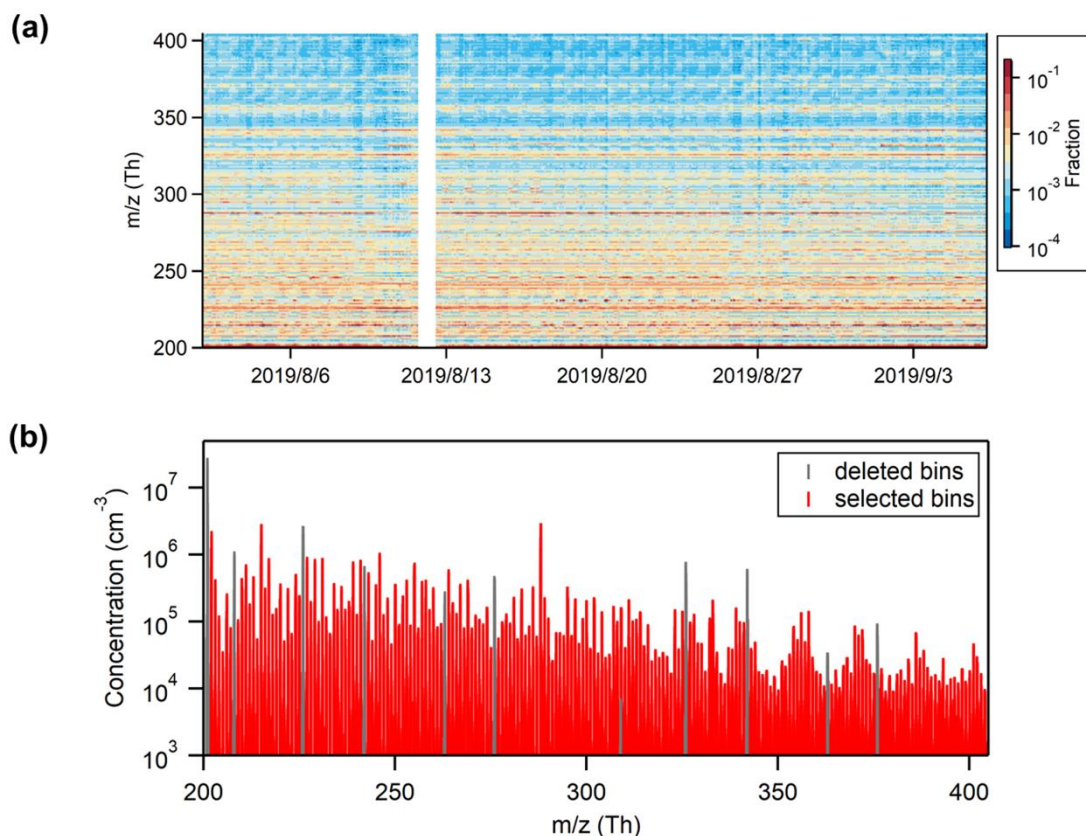


Fig. S2. (a) Normalized mass spectra of nitrate CI-APi-TOF with m/z in the range of 202-404 Th. (b) Averaged binned spectrum measured by nitrate CI-APi-TOF. After delete some bins (gray) affected by compounds listed in Table S1, remaining bins (red) with unit m/z in the range of 202-404 Th were adopted as data matrix for PMF inputs.

S2.2 Evolution

As mentioned in previous classic works applying PMF (Zhang et al., 2011; Yan et al., 2016), the choice of the proper number of factors is the most critical decision towards interpreting the PMF results. When the number of factors solved exceeds 8, the rates of decrease in Q/Q_{exp} (Fig. S2 (a)) and of increase in absolute values (Fig. S2(c)) slow down. A variable should be regarded as explained only if the UEV for that variable is less than 25 % (Fig. S2 (b)). These mathematical diagnostics give us solutions with 9-20 factors to choose from. Solution of more factors can explain more subtle variations in the data, but too many factors can split a physically meaningful factor into unrealistic ones. The evolution of PMF solutions has been carefully viewed, and the first occurrences of main factors are denoted in the corresponding solutions (Fig. S2 (a)). For example, the 'F contaminations' factor, mainly comprising fluorinated

contaminations from perfluorinated acids and Teflon tubing volatiles, first appears purely in the solution of three factors, while the Aliph-OOM factor did not appear until the solution of the 14 factors. Due to the non-uniqueness of the PMF solution, the order of first occurrence of different factors may vary slightly. To some extent, the selection of PMF solutions depends on the interpretability of the factors. From our analysis, solutions with more than 14 factors did not provide new process-specific information and made the interpretability of the results more difficult because of factor splitting and fewer unique correlations with external tracers.

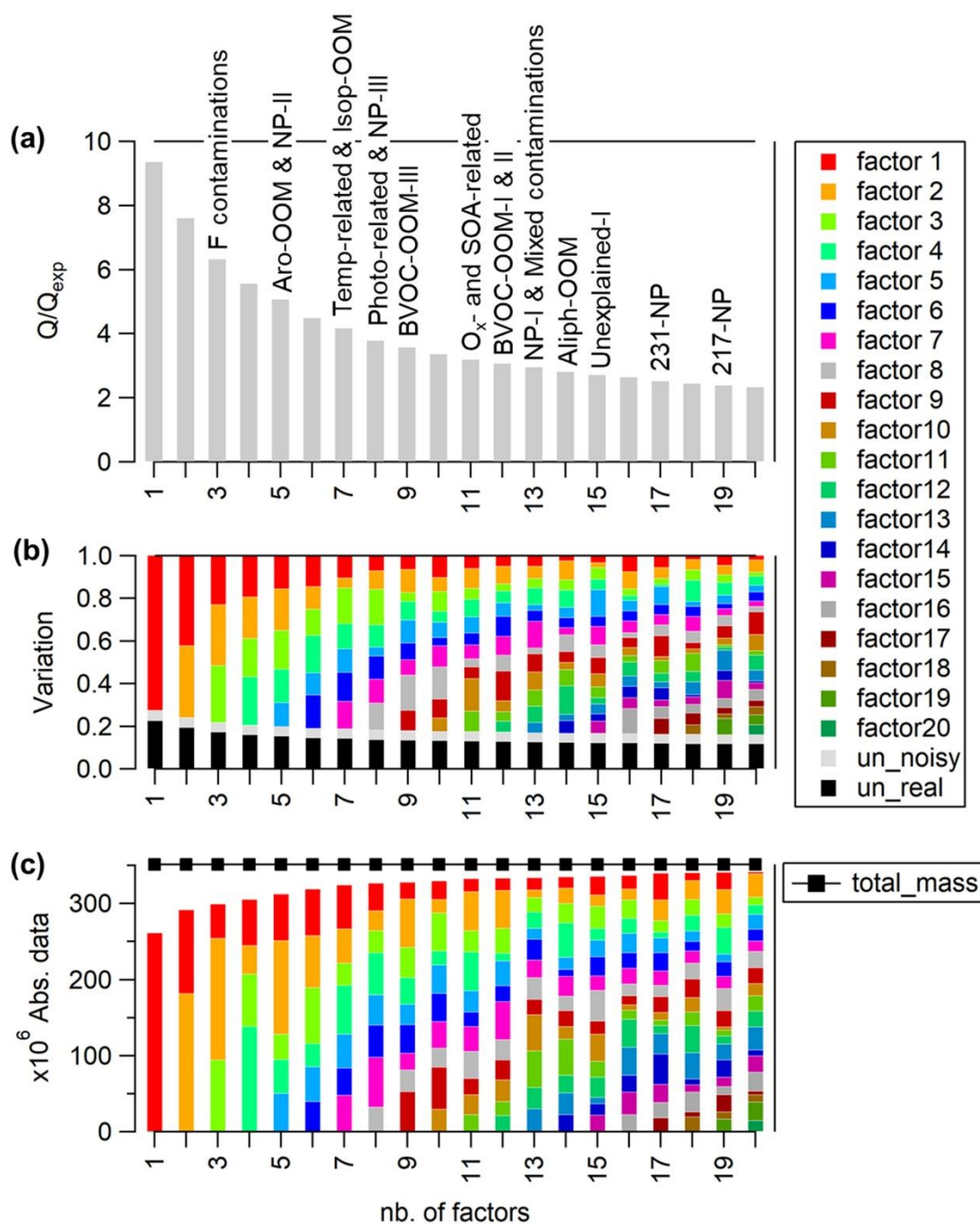


Fig. S3. Diagnostics of PMF solutions, including the evolutions of (a) Q/Q_{exp} , (b) the explained variation (EV) and unexplained variation (UEV), and (c) absolute values

resolved by PMF. In (b) UEV is further separated into the real UEV for data possessing a high signal-to-noise value (un_real) and UEV for noisy data (un_noisy).

S2.3 Rotation

Rotational ambiguity of PMF solution with 14 factors has been checked here (Fig. S3). We set the f_{peak} to increase from -4.0 to 4.0 with a difference of 0.2, for the global control of such rotations. All solutions are divided into two types, one containing 13 + ‘Mixed contaminations’ factors and the other containing 13 + ‘Unexplained I’ factors, with the former occurring more frequently. The ‘Mixed contaminations’ factor consists of mainly by nitrated phenols and fluorinated contaminations, and is negatively correlated with the ‘F contaminations’ factor (Fig. S5), meaning these two factors are somewhat over split. The ‘Unexplained I’ factor has no correlation with external tracer data, and seems to abstract some signal from the Temp-related factor, but peaks at around 17:30 in its diurnal pattern. Finally, the solution with a f_{peak} value of -0.2 is selected to analysis data.

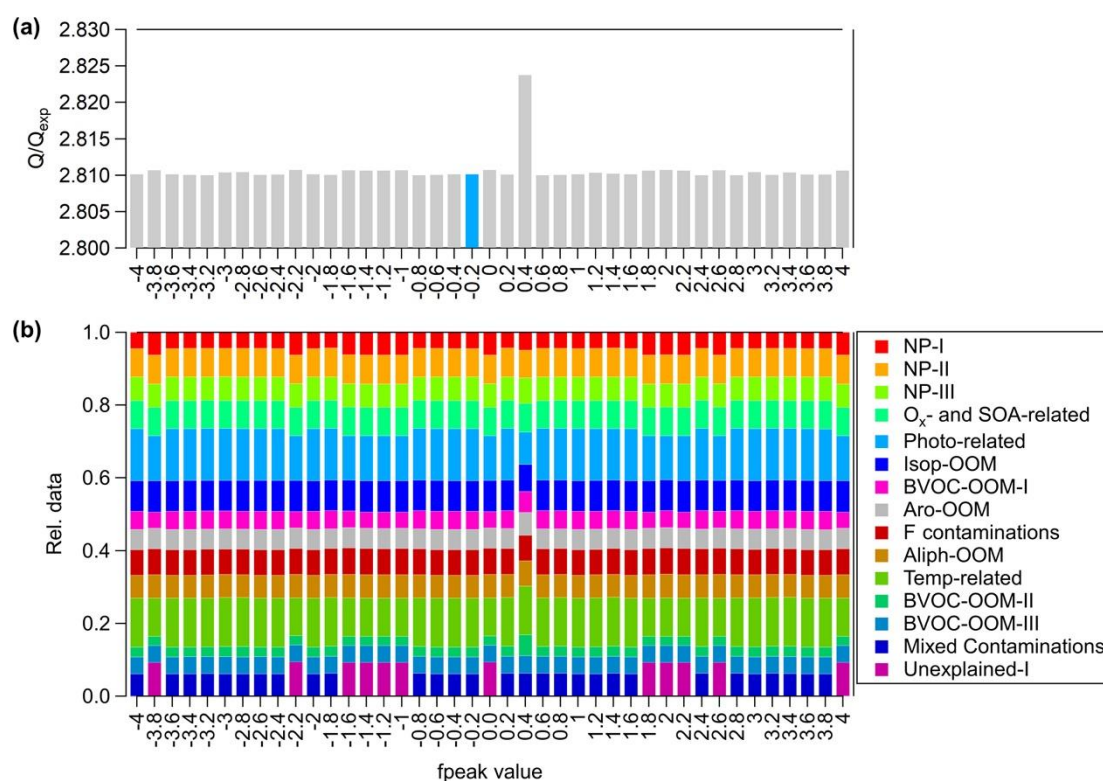


Fig. S4. (a) Q/Q_{exp} distribution on rotation of 14-factors solutions, the one with an f_{peak} value of -0.2 is the selected solution. (b) The relative contribution ratio of factors in each solution with different values of f_{peak} .

S2.4 Residual

The residual histograms are an easy and fast method for investigating whether the PMF result contains some systematic under- or overestimation. As showed in Fig. S4, the

time series of residuals looks full of noise, and dihydroxy nitro-benzene ($C_6H_5NO_4$, charged by NO_3^- at unit m/z 217 Th) and dihydroxy nitro-toluene ($C_7H_7NO_4$, charged by NO_3^- at unit m/z 231 Th) are the largest peaks in mass spectra of residuals. But these two compounds will be distributed to two different factors about nitrated phenols, in the solutions of 17-20 factors (denoted as '217-NP' and '231-NP' factors in Fig. S2 (a)). In order to separate out these two factors, the other physically meaningful factors will be over-split. Since the factors about nitrated phenols are not our main concern, it's reasonable to choose the 14-factors solution.

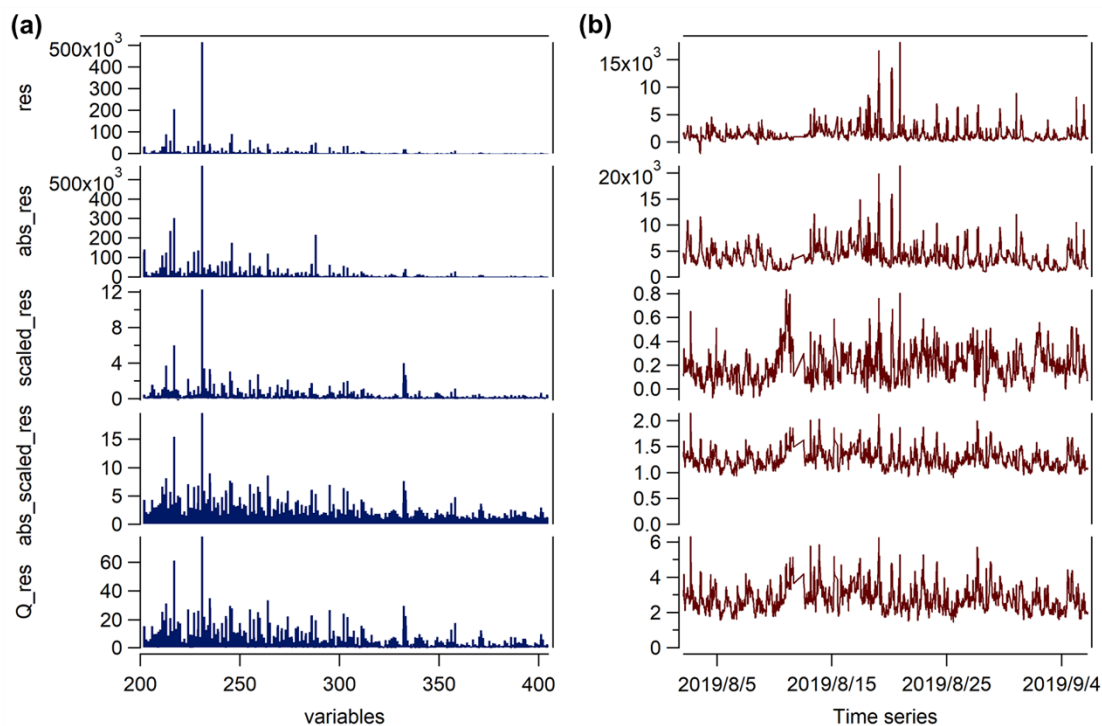


Fig. S5. (a) Mass spectra and (b) time series plots showing the residual histograms of the solution selected.

S2.5 Comparison between the factors

- 1: Temp-related 2: NP-III 3: BVOC-OOM-II 4: Aro-OOM 5: O_x- and SOA-related 6: NP-I
 7: Aliph-OOM 8: BVOC-OOM-III 9: F contaminations 10: Photo-related 11: Isop-OOM
 12: Mixed contaminations 13: NP-II 14: BVOC-OOM-I

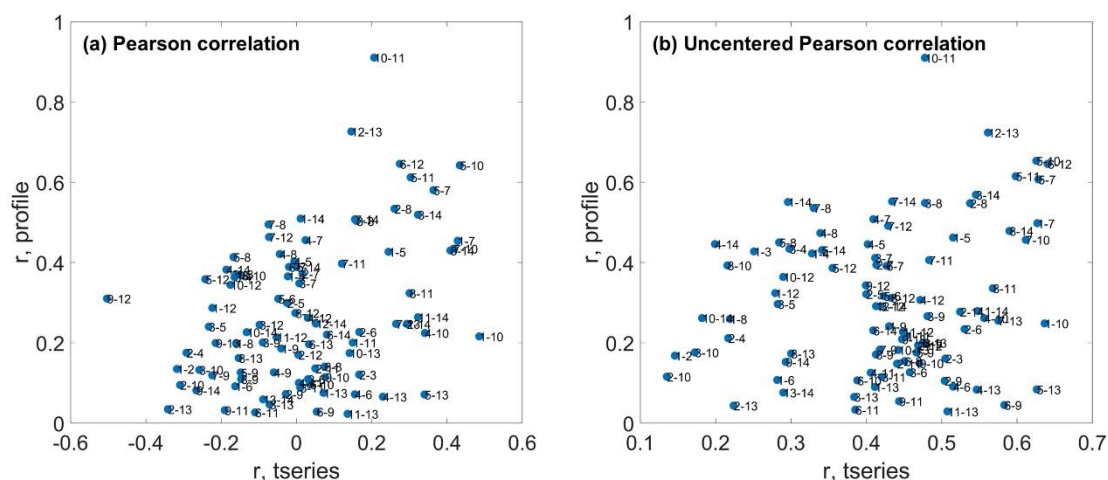


Fig. S6. Comparison among the factors through (a) Pearson correlation and (b) Uncentered Pearson correlation. The x-axis shows the correlation of the time series between the factors, and the y-axis shows the correlation of the spectra between the factors.

S3 Calculation of molecular properties of OOMs

Carbon oxidation state (OS_c)

The OS_c of each **non-nitro** OOM was calculated based on Eq. (3) modified from that in Kroll et al. (2011) include organic nitrate contributions, by assuming that all nitrogen come from the nitrate group (-ONO₂), which are more likely to be detected by the nitrate CI-APi-TOF. A group oxidation state of -1 was applied to -ONO₂ functionality:

$$OS_c = 2(n_O - 3n_N)/n_C - n_H/n_C + n_N/n_C \quad (3)$$

Where n_C , n_H , n_O , and n_N denote the number of carbons, hydrogen, oxygen, and nitrogen in the molecule, respectively. The formula is only valid when $n_O \geq 3 \times n_N$, meaning that there is enough oxygen to account for the -ONO₂ group. Almost all of fitted HR peaks satisfy this condition, further indicating that the detected nitrogen is likely to occur entirely in the -ONO₂ group. However, it is worth mentioning that polyfunctional nitrogenous species with reduced N functionalities (i.e., heterocyclic, amine or nitrite) can still be detected by the nitrate CI-APi-TOF if they contain sufficient oxygenated functional groups (e.g., -OH, -OOH).

Double bond equivalent (DBE)

The DBE of each OOM was calculated using Eq. (4), by assuming that all nitrogen come from the nitrate group (-ONO₂) or nitro group (-NO₂). Here DBE represents the combined effect of double or triple bonds, as well as the ring structure, in the molecule.

$$\text{DBE} = n_{\text{C}} + 1 - (n_{\text{H}} + n_{\text{N}})/2 \quad (4)$$

Volatility Basis Set (VBS)

The saturation concentration (volatility) of selected OOMs was estimated based on the group-contribution method proposed by Donahue et al. (2011):

$$\log_{10}C^*(300\text{K}) = (25 - n_{\text{C}}) \cdot b_{\text{C}} - (n_{\text{O}} - 2n_{\text{N}}) \cdot b_{\text{O}} - 2 \left[\frac{(n_{\text{O}} - 2n_{\text{N}}) \cdot n_{\text{C}}}{n_{\text{C}} + n_{\text{O}} - 2n_{\text{N}}} \right] \cdot b_{\text{CO}} \quad (5)$$

Where $b_{\text{C}} = 0.475$, $b_{\text{O}} = 2.3$, $b_{\text{CO}} = -0.3$. The effect of nitrate group (-ONO₂) on volatility is similar to hydroxyl group (-OH).

The temperature dependence of volatilities is described by Eq. (6), according to Stolzenburg et al. (2018):

$$\log_{10}C_i^*(T) = \log_{10}C_i^*(300\text{K}) + \frac{\Delta H_{\text{vap}}}{R \cdot \ln(10)} \left(\frac{1}{300} - \frac{1}{T} \right) \quad (6)$$

The evaporation enthalpy (ΔH_{vap}) can be linked to the saturation mass concentration at 300 K, $\log_{10} C^*(300\text{K})$, according to Donahue et al. (2011) and combined with Epstein et al. (2010):

$$\Delta H_{\text{vap}}[\text{kJ mol}^{-1}] = 129 - 5.7 \cdot \log_{10}(C^*(300\text{K})) \quad (7)$$

S4 Main peaks of 9 discussed non-nitrated-phenols factors

S4.1 Aro-OOM factor

Table S2. Molecular characteristics of the Aro-OOM factor. Presented as several sets of compounds, and the members of each sets differ in the addition of a -CH₂ moiety. Only the signals that account for more than one thousandth of the factor are selected to reduce uncertainties. The clustering reagent ion NO₃⁻ or HNO₃NO₃⁻ has been omitted from the formulas.

No.	Formulas	Contribution to the factor (%)	DBE	no	nN
1	$C_xH_{2x-1}O_6N$, x= [3, 14]	11.0	1	6	1
2	$C_xH_{2x-7}O_4N$, x= [6, 8]	6.2	4	4	1 ^a
3	$C_xH_{2x-3}O_6N$, x= [5, 15]	5.3	2	6	1
4	$C_xH_{2x-4}O_4$, x= [6, 11]	4.6	3	4	0
5	$C_xH_{2x-3}O_7N$, x= [6, 13]	3.5	2	7	1
6	$C_xH_{2x-5}O_7N$, x= [7, 14]	3.5	3	7	1
7	$C_xH_{2x-5}O_8N$, x= [8, 13]	2.9	3	8	1
8	$C_xH_{2x-4}O_5$, x= [5, 12]	2.9	3	5	0
9	$C_xH_{2x-5}O_6N$, x= [6, 12]	2.8	3	6	1
10	$C_xH_{2x-2}O_4$, x= [6, 10]	2.7	2	6	0

a. The nitrogen atom comes from the nitro functional group.

S4.2 Temp-related factor

Table S3. Molecular characteristics of the Temp-related factor. Presented as several sets of compounds, and the members of each sets differ in the addition of a $-CH_2$ moiety. Only the signals that account for more than one thousandth of the factor are selected to reduce uncertainties. The clustering reagent ion NO_3^- or $HNO_3NO_3^-$ has been omitted from the formulas.

No.	Formulas	Contribution to the factor (%)	DBE	no	nN
1	$C_xH_{2x-4}O_5$, x= [5, 11]	10.0	3	5	0
2	$C_xH_{2x-2}O_5$, x= [5, 10]	7.8	2	5	0
3	$C_xH_{2x-1}O_6N$, x= [3, 7]	6.0	1	6	1
4	$C_xH_{2x-6}O_5$, x= [5, 11]	5.4	4	5	0
5	$C_xH_{2x-4}O_6$, x= [5, 10]	5.3	3	6	0
6	$C_xH_{2x-3}O_7N$, x= [4, 10]	5.0	2	7	1
7	$C_xH_{2x-3}O_6N$, x= [4, 9]	4.3	2	6	1
8	$C_xH_{2x-1}O_7N$, x= [4, 9]	2.9	1	7	1
9	$C_xH_{2x-4}O_4$, x= [6, 9]	2.3	4	4	0
10	$C_xH_{2x-6}O_6$, x= [7, 11]	2.1	4	6	0

S4.3 Aliph-OOM factor

Table S4. Molecular characteristics of the Aliph-OOM factor. Presented as several sets of compounds, and the members of each sets differ in the addition of a $-CH_2$ moiety. Only the signals that account for more than one thousandth of the factor are selected to reduce uncertainties. The clustering reagent ion NO_3^- or $HNO_3NO_3^-$ has been omitted

from the formulas.

No.	Formulas	Contribution to the factor (%)	DBE	no	n _N
1	C _x H _{2x-3} O ₆ N, x= [4, 12]	10.0	2	6	1
2	C _x H _{2x-2} O ₈ N ₂ , x= [4, 13]	9.0	1	8	2
3	C _x H _{2x-3} O ₇ N, x= [5, 12]	5.9	2	7	1
4	C _x H _{2x-1} O ₆ N, x= [3, 11]	5.7	1	6	1
5	C _x H _{2x-1} O ₅ N, x= [4, 9]	4.9	1	5	1
6	C _x H _{2x} O ₈ N ₂ , x= [4, 9]	3.4	0	8	2
7	C _x H _{2x-5} O ₇ N, x= [6, 13]	2.8	3	7	1
8	C _x H _{2x-4} O ₄ , x= [6, 10]	2.8	3	4	0
9	C _x H _{2x} O ₇ N ₂ , x= [4, 11]	2.2	0	7	2
10	C _x H _{2x-4} O ₅ , x= [5, 11]	2.2	3	5	0

S4.4 Photo-related factor

Table S5. Molecular characteristics of the Photo-related factor. Presented as several sets of compounds, and the members of each sets differ in the addition of a -CH₂ moiety. Only the signals that account for more than one thousandth of the factor are selected to reduce uncertainties. The clustering reagent ion NO₃⁻ or HNO₃NO₃⁻ has been omitted from the formulas.

No.	Formulas	Contribution to the factor (%)	DBE	no	n _N
1	C _x H _{2x} O ₈ N ₂ , x= [5]	18.0	0	8	2
2	C _x H _{2x-3} O ₇ N, x= [4, 11]	6.5	2	7	1
3	C _x H _{2x-1} O ₆ N, x= [3, 10]	6.3	1	6	1
4	C _x H _{2x-7} O ₄ N, x= [6, 8]	3.6	4	4	1 ^b
5	C _x H _{2x-7} O ₃ N, x= [7, 8] ^a	3.3	4	3	1 ^b
6	C _x H _{2x-5} O ₇ N, x= [5, 11]	2.5	3	7	1
7	C _x H _{2x-4} O ₁₀ N ₂ , x= [7, 10]	2.2	2	10	2
8	C _x H _{2x-3} O ₈ N, x= [5, 10]	2.1	2	8	1
9	C _x H _{2x-5} O ₈ N, x= [6, 11]	2.1	3	8	1
10	C _x H _{2x-4} O ₅ , x= [5, 8]	2.0	3	5	0

a. Do not contain nitro phenol with a carbon number of 6, because we removed it before binPMF. b. The nitrogen atom comes from the nitro functional group.

S4.5 O_x- and SOA-related factor

Table S6. Molecular characteristics of the O_x- and SOA-related factor. Presented as several sets of compounds, and the members of each sets differ in the addition of a -

CH₂ moiety. Only the signals that account for more than one thousandth of the factor are selected to reduce uncertainties. The clustering reagent ion NO₃⁻ or HNO₃NO₃⁻ has been omitted from the formulas.

No.	Formulas	Contribution to the factor (%)	DBE	no	nN
1	C _x H _{2x-7} O ₃ N, x= [6, 8]	7.5	4	3	1 ^a
2	C _x H _{2x} O ₈ N ₂ , x= [5]	6.4	0	8	2
3	C _x H _{2x-1} O ₆ N, x= [3, 9]	6.3	1	6	1
4	C _x H _{2x-3} O ₆ N, x= [4, 9]	6.2	2	6	1
5	C _x H _{2x-2} O ₈ N ₂ , x= [4, 10]	4.7	1	8	2
6	C _x H _{2x-6} O ₅ , x= [6, 10]	3.5	4	5	0
7	C _x H _{2x-7} O ₄ N, x= [6, 8]	3.5	4	4	1 ^a
8	C _x H _{2x-4} O ₅ , x= [5, 9]	2.9	3	5	0
9	C _x H _{2x-5} O ₇ N, x= [5, 10]	2.5	3	7	1
10	C _x H _{2x-1} O ₁₀ N ₃ , x= [5]	1.7	0	10	3

a. The nitrogen atom comes from the nitro functional group.

S4.6 Isop-OOM factor

Table S7. Molecular characteristics of the Isop-OOM factor. Presented as several sets of compounds, and the members of each sets differ in the addition of a '-O' moiety. Only the signals that account for more than one thousandth of the factor are selected to reduce uncertainties. The clustering reagent ion NO₃⁻ or HNO₃NO₃⁻ has been omitted from the formulas.

No.	Formulas	Contribution to the factor (%)	DBE	nc	nN
1	C ₅ H ₁₀ O _x N ₂ , x= [7, 8]	30.7	0	5	2
2	C ₄ H ₇ O _x N, x= [5, 6]	9.0	1	4	1
3	C ₅ H ₉ O _x N, x= [4, 7]	8.8	1	5	1
4	C ₅ H ₇ O _x N, x= [5, 8]	4.6	2	5	1
5	C ₅ H ₈ O _x N ₂ , x= [6, 9]	3.6	1	5	2
6	C ₅ H ₁₁ O _x N, x= [5, 6]	3.5	0	5	1
7	C ₅ H ₉ O _x N ₃ , x= [10]	2.5	0	5	3

S4.7 BVOC-OOM-I factor

Table S8. Molecular characteristics of the BVOC-OOM-I factor. Presented as several sets of compounds, and the members of each sets differ in the addition of a '-O' moiety. Only the signals that account for more than one thousandth of the factor are selected to reduce uncertainties. The clustering reagent ion NO₃⁻ or HNO₃NO₃⁻ has been omitted from the formulas.

No.	Formulas	Contribution to the factor (%)	DBE	nc	nN
1	C ₅ H ₉ O _x N, x= [4, 8]	6.0	1	5	1
2	C ₅ H ₁₀ O _x N ₂ , x= [7, 10]	4.1	0	5	2
3	C ₉ H ₁₅ O _x N, x= [6, 9]	3.6	2	9	1
4	C ₁₀ H ₁₅ O _x N, x= [6, 11]	3.6	3	10	1
5	C ₅ H ₇ O _x N, x= [5, 8]	3.4	2	5	1
6	C ₅ H ₈ O _x N ₂ , x= [7, 10]	3.3	1	5	2
7	C ₆ H ₁₁ O _x N, x= [5, 9]	2.9	1	6	1
8	C ₆ H ₉ O _x N, x= [5, 8]	2.7	2	6	1
9	C ₄ H ₇ O _x N, x= [5, 6]	2.7	1	4	1
10	C ₇ H ₉ O _x N, x= [6, 8]	2.5	3	7	1

S4.8 BVOC-OOM-II factor

Table S9. Molecular characteristics of the BVOC-OOM-II factor. Presented as several sets of compounds, and the members of each sets differ in the addition of a '-O' moiety. Only the signals that account for more than one thousandth of the factor are selected to reduce uncertainties. The clustering reagent ion NO₃⁻ or HNO₃NO₃⁻ has been omitted from the formulas.

No.	Formulas	Contribution to the factor (%)	DBE	nc	nN
1	C ₁₀ H ₁₅ O _x N, x= [5, 12]	9.8	3	10	1
2	C ₁₀ H ₁₇ O _x N, x= [5, 10]	4.4	2	10	1
2	C ₇ H ₉ O _x N, x= [6, 8]	4.2	3	7	1
4	C ₉ H ₁₅ O _x N, x= [6, 9]	3.7	2	9	1
5	C ₁₀ H ₁₆ O _x N, x= [6, 11]	3.3	2.5	10	1
6	C ₁₀ H ₁₆ O _x N ₂ , x= [7, ,11]	2.5	2	10	2
7	C ₉ H ₁₃ O _x N, x= [6, 10]	2.2	3	9	1
8	C ₅ H ₈ O _x N, x= [5]	2.1	1.5	5	1
9	C ₈ H ₁₃ O _x N, x= [6, 8]	1.7	2	8	1
10	C ₆ H ₁₁ O _x N, x= [6, 8]	1.6	1	6	1

S4.9 BVOC-OOM-III factor

Table S10. Molecular characteristics of the BVOC-OOM-III factor. Presented as several sets of compounds, and the members of each sets differ in the addition of a '-O' moiety. Only the signals that account for more than one thousandth of the factor are selected to reduce uncertainties. The clustering reagent ion NO₃⁻ or HNO₃NO₃⁻ has been omitted from the formulas.

No.	Formulas	Contribution to the factor (%)	DBE	nc	nN
1	C ₁₀ H ₁₅ O _x N, x= [5, 9]	7.1	3	10	1
2	C ₈ H ₁₁ O _x N, x= [6, 8]	4.5	3	8	1
3	C ₉ H ₁₅ O _x N, x= [5, 8]	4.4	2	9	1
4	C ₁₀ H ₁₆ O _x N ₂ , x= [7, 10]	4.1	2	10	2
5	C ₁₀ H ₁₇ O _x N, x= [5, 8]	3.9	2	10	1
6	C ₆ H ₄ O _x N ₂ , x= [5]	3.8	4	6	2 ^a
7	C ₇ H ₁₁ O _x N, x= [5, 7]	3.0	2	7	1
8	C ₅ H ₁₀ O _x N ₂ , x= [8]	2.8	0	5	2
9	C ₁₀ H ₁₈ O _x N ₂ , x= [7, 10]	2.6	1	10	2
10	C ₉ H ₁₃ O _x N, x=[5, 8]	2.4	3	9	1

a. The nitrogen atom comes from the nitro functional group.

S5 The dependence of Temp-related factor on temperature

The total concentration of this factor in the gas and aerosol phases was calculated considering the effect of temperature on gas-particle partitioning (Eq. 8), so that we can investigate the possible formation mechanisms from the correlation analysis of Fig. S6 (c) and (d).

$$\zeta_i = \left(1 + \frac{C_i^*}{C_{OA}}\right)^{-1} \quad (8)$$

In equation 1, ζ_i represents the partitioning coefficient (the ratio of the concentration of compound i in the condensed phase to its total concentration in the atmosphere), COA is the total mass concentration of organic aerosol, and C_i^* represents the saturation concentration of compound i.

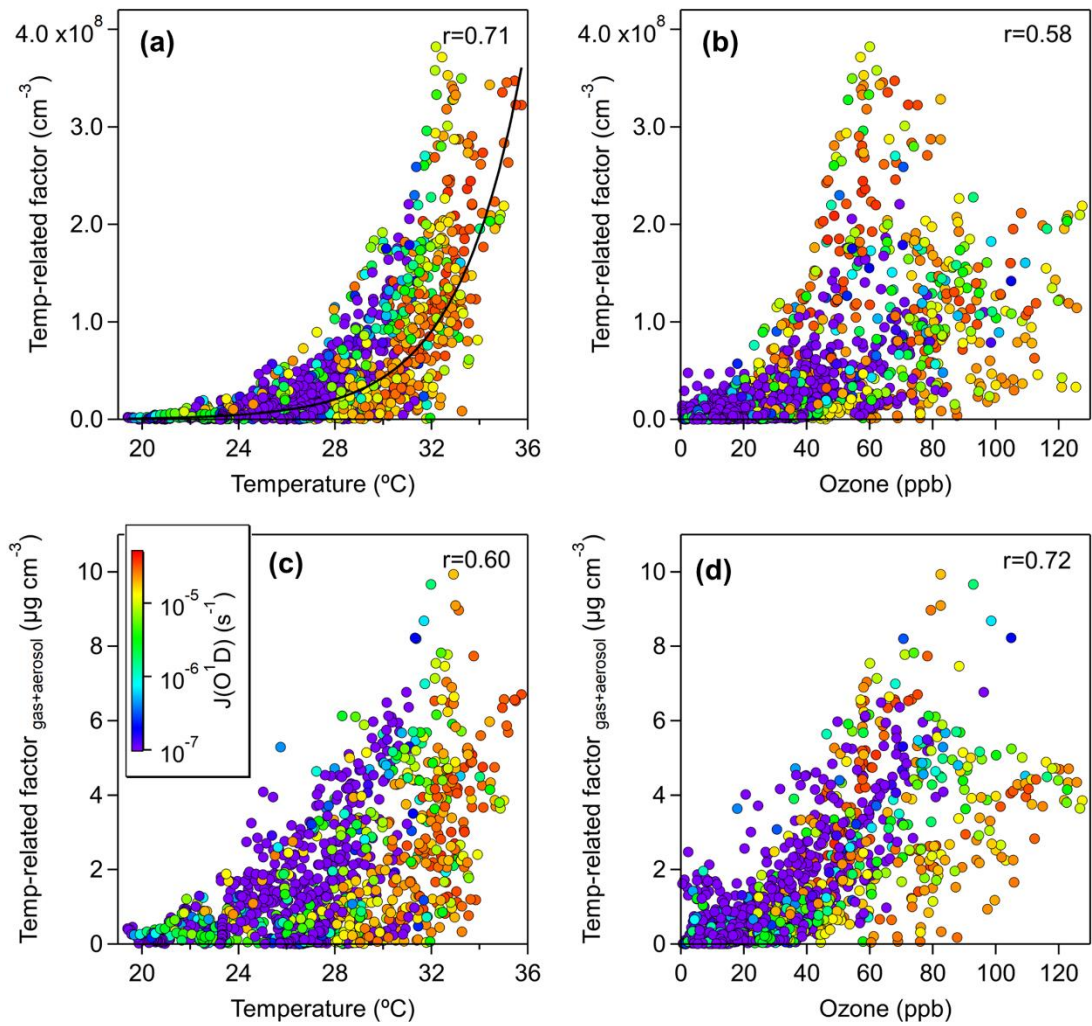


Figure S7. Scatter plots of Temp-related factor with (a) temperature, (b) ozone, the solid black curve in (a) was obtained by e-exponential fitting. All the scatters are colored by $J(O^1D)$, to show the difference between day and night.

S6 Air masses reaching the SORPES station

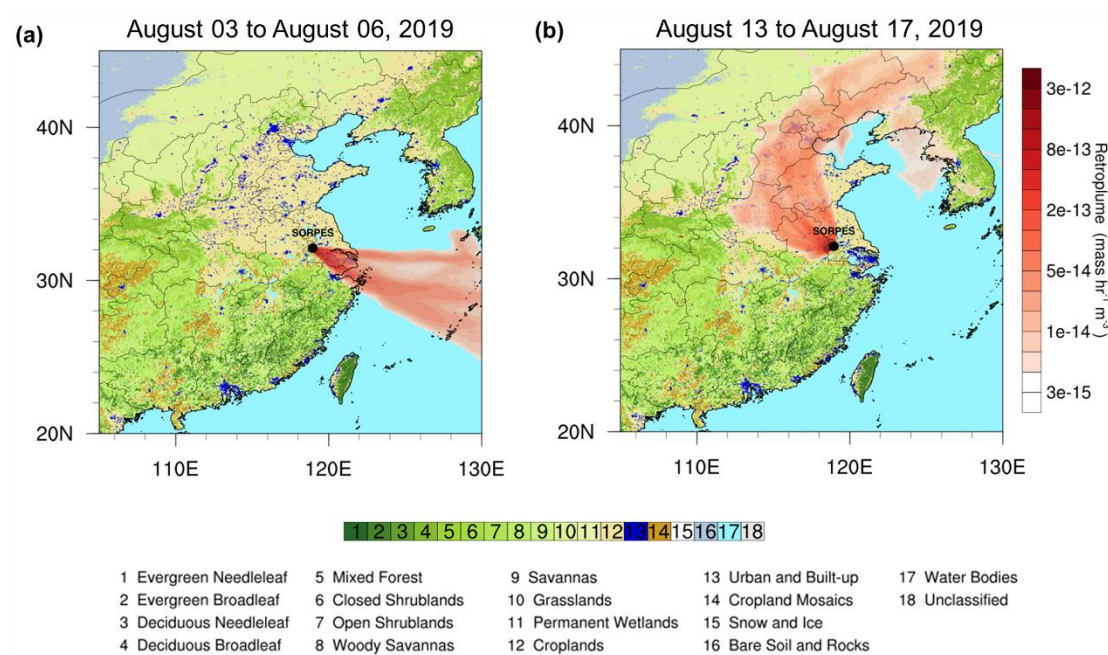


Fig. S8. The averaged retroplumes (i.e., 100 m footprint) based on 3-day backward Lagrangian particle dispersion modeling during (a) August 03 to August 06, 2019, and (b) August 13 to August 17, 2019. Note: Black dot gives the location of the SORPES station. The method of calculating the footprint was developed by (Ding et al., 2013), based on the Hybrid Single-Particle Lagrangian Integrated Trajectory (HYSPLIT) model (Stein et al., 2015). The types of land cover were got from The Terra and Aqua combined Moderate Resolution Imaging Spectroradiometer (MODIS) Land Cover Type (MCD12Q1) (<https://lpdaac.usgs.gov/products/mcd12q1v006/>, last access: 11 March 2021).

S7 High resolution peak fitting

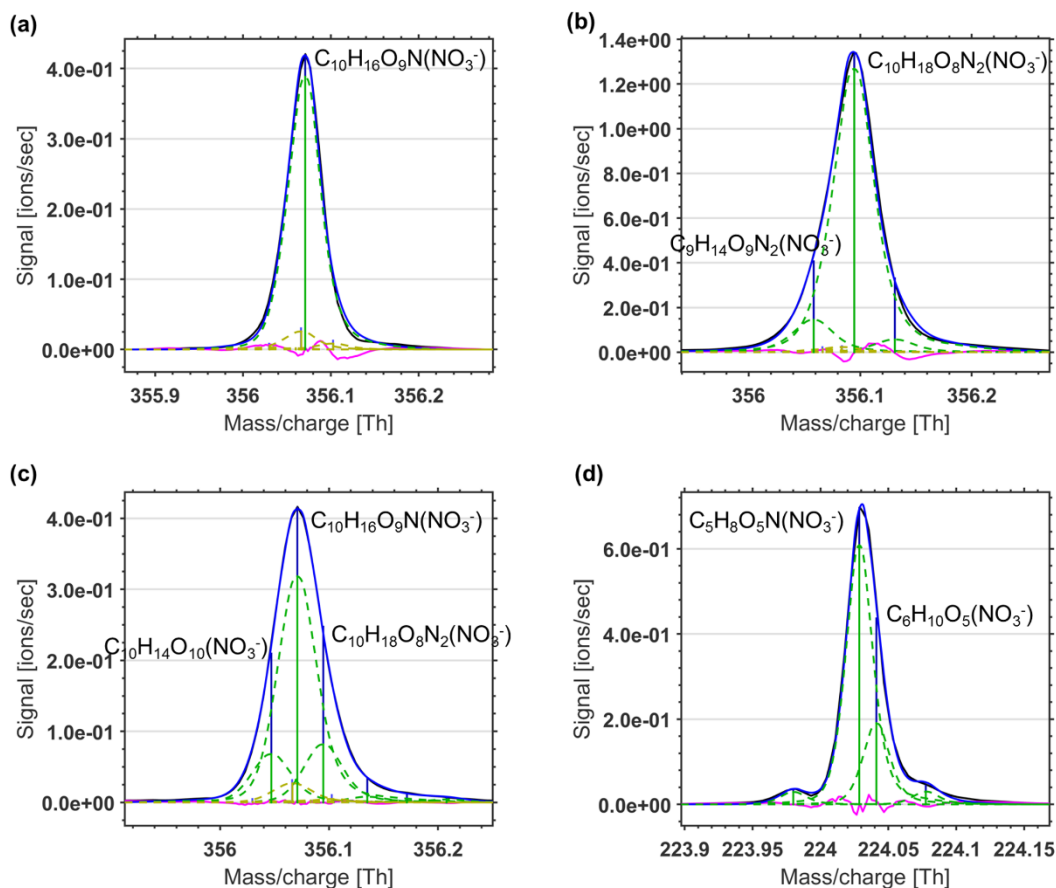


Fig. S9. Examples of peak fitting. Peaks of unit m/z at 356 Th in (a) the BVOC-OOM-I factor, (b) the BVOC-OOM-III factor, and (c) the BVOC-OOM-II factor. Peaks of unit m/z at 224 Th in (d) the BVOC-OOM-II factor. The black solid line is the measured signal, the blue solid line is the total signal of the fitted peaks, the green dashed line denotes the fitted peak, and the purple one is the residual.

Reference

Ding, A., Wang, T., and Fu, C.: Transport characteristics and origins of carbon monoxide and ozone in Hong Kong, South China, *Journal of Geophysical Research: Atmospheres*, 118, 9475-9488, <https://doi.org/10.1002/jgrd.50714>, 2013.

Donahue, N. M., Epstein, S. A., Pandis, S. N., and Robinson, A. L.: A two-dimensional volatility basis set: 1. organic-aerosol mixing thermodynamics, *Atmospheric Chemistry and Physics*, 11, 3303-3318, 10.5194/acp-11-3303-2011, 2011.

Epstein, S. A., Riipinen, I., and Donahue, N. M.: A Semiempirical Correlation between Enthalpy of Vaporization and Saturation Concentration for Organic Aerosol, *Environmental Science & Technology*, 44, 743-748, 10.1021/es902497z, 2010.

Kroll, J. H., Donahue, N. M., Jimenez, J. L., Kessler, S. H., Canagaratna, M. R., Wilson, K. R., Altieri, K. E., Mazzoleni, L. R., Wozniak, A. S., Bluhm, H., Mysak, E. R., Smith, J. D., Kolb, C. E., and Worsnop, D. R.: Carbon oxidation state as a metric for describing

the chemistry of atmospheric organic aerosol, *Nature Chemistry*, 3, 133-139, 10.1038/nchem.948, 2011.

Polissar, A. V., Hopke, P. K., Paatero, P., Malm, W. C., and Sisler, J. F.: Atmospheric aerosol over Alaska: 2. Elemental composition and sources, *Journal of Geophysical Research: Atmospheres*, 103, 19045-19057, <https://doi.org/10.1029/98JD01212>, 1998.

Stein, A. F., Draxler, R. R., Rolph, G. D., Stunder, B. J. B., Cohen, M. D., and Ngan, F.: NOAA's HYSPLIT Atmospheric Transport and Dispersion Modeling System, *Bulletin of the American Meteorological Society*, 96, 2059-2077, 10.1175/BAMS-D-14-00110.1, 2015.

Stolzenburg, D., Fischer, L., Vogel, A. L., Heinritzi, M., Schervish, M., Simon, M., Wagner, A. C., Dada, L., Ahonen, L. R., Amorim, A., Baccharini, A., Bauer, P. S., Baumgartner, B., Bergen, A., Bianchi, F., Breitenlechner, M., Brilke, S., Mazon, S. B., Chen, D., Dias, A., Draper, D. C., Duplissy, J., El Haddad, I., Finkenzeller, H., Frege, C., Fuchs, C., Garmash, O., Gordon, H., He, X., Helm, J., Hofbauer, V., Hoyle, C. R., Kim, C., Kirkby, J., Kontkanen, J., Kuerten, A., Lampilahti, J., Lawler, M., Lehtipalo, K., Leiminger, M., Mai, H., Mathot, S., Mentler, B., Molteni, U., Nie, W., Nieminen, T., Nowak, J. B., Ojdanic, A., Onnela, A., Passananti, M., Petaja, T., Quelever, L. L. J., Rissanen, M. P., Sarnela, N., Schallhart, S., Tauber, C., Tome, A., Wagner, R., Wang, M., Weitz, L., Wimmer, D., Xiao, M., Yan, C., Ye, P., Zha, Q., Baltensperger, U., Curtius, J., Dommen, J., Flagan, R. C., Kulmala, M., Smith, J. N., Worsnop, D. R., Hansel, A., Donahue, N. M., and Winkler, P. M.: Rapid growth of organic aerosol nanoparticles over a wide tropospheric temperature range, *Proc. Natl. Acad. Sci. U. S. A.*, 115, 9122-9127, 10.1073/pnas.1807604115, 2018.

Yan, C., Nie, W., Äijälä, M., Rissanen, M. P., Canagaratna, M. R., Massoli, P., Junninen, H., Jokinen, T., Sarnela, N., Häme, S. A. K., Schobesberger, S., Canonaco, F., Yao, L., Prévôt, A. S. H., Petäjä, T., Kulmala, M., Sipilä, M., Worsnop, D. R., and Ehn, M.: Source characterization of highly oxidized multifunctional compounds in a boreal forest environment using positive matrix factorization, *Atmospheric Chemistry and Physics*, 16, 12715-12731, 10.5194/acp-16-12715-2016, 2016.

Zhang, Q., Jimenez, J. L., Canagaratna, M. R., Ulbrich, I. M., Ng, N. L., Worsnop, D. R., and Sun, Y.: Understanding atmospheric organic aerosols via factor analysis of aerosol mass spectrometry: a review, *Anal Bioanal Chem*, 401, 3045-3067, 10.1007/s00216-011-5355-y, 2011.

Zhang, Y., Peräkylä, O., Yan, C., Heikkinen, L., Äijälä, M., Daellenbach, K. R., Zha, Q., Riva, M., Garmash, O., Junninen, H., Paatero, P., Worsnop, D., and Ehn, M.: A novel approach for simple statistical analysis of high-resolution mass spectra, *Atmos. Meas. Tech.*, 12, 3761-3776, 10.5194/amt-12-3761-2019, 2019.